WARSAW UNIVERSITY OF TECHNOLOGY Index 351733
FACULTY OF CIVIL ENGINEERING
COMMITTEE FOR CIVIL AND WATER ENGINEERING
POLISH ACADEMY OF SCIENCES ISSN 1230-2945

DOI: 10.24425/ace.2025.155104
ARCHIVES OF CIVIL ENGINEERING
Vol. LXXI ISSUE 3 2025
pp. 355–368



**Research paper**

# Influence of steel fiber content on the frost resistance of steel fiber reinforced rubberized concrete in sulfate environment

**Lei Jiang[1], Ming Zhang[2], Jiahua Jing[3]**

**Abstract:** To evaluate the performance of steel fiber-reinforced rubber concrete (SFRRC) in a sulfate environment, a rapid freeze-thaw testing procedure was employed to assess the influence of steel fiber content on parameters such as mass, relative dynamic modulus of elasticity, compressive strength, and damage layer thickness ($H_f$) of SFRRC. The testing revealed the deterioration pattern of SFRRC in a sulfate erosion and freeze-thaw environment. Additionally, the mercury intrusion porosimetry technique was utilized to further investigate the pore structure characteristics of SFRRC with the goal of revealing the damage mechanism from a microscopic perspective. The results indicate that SFRRC undergoes a lower degree of freeze-thaw damage in sulfate solution than rubber concrete without steel fibers. The degree of deterioration of SFRRC gradually decreases with an increasing steel fiber content, but its frost resistance is adversely affected at a content level of 2.0%. The $H_f$ can be used to characterize the internal damage in the SFRRC. As the $H_f$ increases, the loss of compressive strength in the damage layer becomes more pronounced. A correlation exists between the compressive strength of SFRRC and that of the damage layer under sulfate erosion and freeze-thaw conditions, enabling calculation of the latter based on the compressive strength of the SFRRC under the influence of environmental factors. An appropriate incorporation of steel fibers optimizes the pore structure of SFRRC. As the steel fiber content gradually increases within a range of 0 to 1.5%, the total porosity decreases along with the total pore volume and area. This leads to an improvement in the pore structure of the SFRRC. At a content of 1.5%, the pore structure of SFRRC is optimized and its resistance to sulfate freeze-thaw performance is maximized.

**Keywords:** damage layer thickness, freeze-thaw cycling, pore structure, steel fiber reinforced rubberized concrete, sulfate erosion

[1]PhD., College of Civil Engineering and Architecture, Anyang Normal University, Anyang 455000, China, Engineering Technology Research Center of Henan Province for Digital Intelligent Building and Low Carbon Building Material, Anyang 455000, China e-mail: aynujianglei@163.com, ORCID: 0009-0008-3622-5363
[2]PhD., College of Civil Engineering and Architecture, Anyang Normal University, Anyang 455000, China; Engineering Technology Research Center of Henan Province for Digital Intelligent Building and Low Carbon Building Material, Anyang 455000, China, e-mail: aynuzhangming@163.com, ORCID: 0000-0001-9248-0619
[3]PhD., College of Civil Engineering and Architecture, Anyang Normal University, Anyang 455000, China; Engineering Technology Research Center of Henan Province for Digital Intelligent Building and Low Carbon Building Material, Anyang 455000, China, e-mail: jingjiahua@aynu.edu.cn, ORCID: 0009-0000-4542-901X

# 1. Introduction

Due to the rapid growth of the global automotive and rubber industries, there has been a consistent increase in the quantity of discarded tires and rubber products. The substantial accumulation of discarded rubber resulting from its slow degradation and the low efficiency of resource utilization has led to significant resource wastage and environmental pollution. Rubberized concrete is a novel, environmentally friendly building material produced by the incorporation of particles or powder derived from discarded rubber into concrete. This material can address some of the land occupation and environmental impact issues caused by discarded rubber [1, 2]. However, research has revealed that the incorporation of rubber particles into the cementitious matrix of rubberized concrete faces challenges in terms of high porosity arising from factors such as poor adhesion and the introduction of gas during mixing. Because this can reduce concrete strength, the widespread adoption of rubberized concrete has been limited [3,4].

The incorporation of fibers has emerged as a common method for enhancing the properties of concrete. This encompasses the addition of various individual fiber types, including steel, polypropylene, basalt, or other fibers, as well as the blending of two or more types of hybrid fibers [5, 6]. Notably, steel fibers, owing to their superior mechanical properties and diverse geometrical shapes, have found extensive application in engineering projects. The addition of steel fiber in rubber concrete has been found to effectively address issues related to strength reduction. Furthermore, this incorporation also contributes towards enhancing the toughness of rubber concrete [7–9].

Pavements, one of the main applicational areas of SFRRC, are constructed on soil foundations and exposed to natural environmental conditions. They are susceptible to the effects of underground corrosive sulfates and temperature variation in cold regions, factors that directly impact the reliability and service life of pavement engineering projects [10, 11]. In recent years, domestic and international research has focused on durability issues of steel fiber or rubber concretes such as freeze-thaw cycling and sulfate erosion [12–16]. However, research on SFRRC has primarily focused on mechanical properties, with limited attention given to durability studies.

Alsaif et al. [17] investigated the degradation of SFRRC in a 3% NaCl solution subjected to wet-dry cycles. The results indicated that there was minimal increase in chloride ion permeation with higher rubber content. After undergoing either a 150 or 300-day dry-wet cycle test, no visible indications of deterioration or surface cracking were observed on the SFRRC specimens. Alsaif et al. [18] also demonstrated that incorporating steel fibers into rubberized concrete with a high rubber content can significantly enhance its frost resistance. The research conducted by Luo et al. [19] demonstrates that the incorporation of steel fibers in rubberized concrete significantly enhances its flexural strength after undergoing 150 freeze-thaw cycles. Additionally, increasing the proportion of steel fibers is found to be associated with a decrease in the mass loss rate of the rubberized concrete. Chen et al. [20] indicated that an increase in the rubber particle content to over 20% results in a higher presence of internal pores within the steel fiber-reinforced recycled concrete, consequently causing reductions in both compressive strength and frost resistance.

Currently, research on the durability of SFRRC primarily focuses on individual environmental factors, with only a few studies addressing its performance under multifactorial environmental conditions. This study focuses on the impact of varying steel fiber content in SFRRC and conducts a comprehensive analysis of the weight loss, alterations in relative dynamic modulus of elasticity (RDME), reduction in compressive strength, and changes in $H_f$ when subjected to a combination of sulfate erosion and freeze-thaw conditions. The degradation patterns observed in SFRRC are also explored based on the results. By considering the evolution law of the damage layer, the mechanical properties of this layer in SFRRC are examined. Furthermore, the results of mercury intrusion porosimetry are utilized to investigate the pore structure characteristics of SFRRC, analyze the impact of steel fiber on the pore structure, and provide a microscopic perspective on damage mechanisms.

# 2. Experiment

## 2.1. Materials and mix proportions

The experiment utilized HuBo brand P·O 42.5 ordinary Portland cement and grade II fly ash sourced from Dadang Power Plant. The fine aggregate comprised ordinary river sand, characterized by a fineness modulus of 2.7, while the coarse aggregate consisted of continuously graded gravel particles ranging from 5 to 20 mm in size. Rubber, with a particle size ranging from 1 to 2 mm and an apparent density of 1050 kg/m$^3$, was used as a fine aggregate. Wave-shaped steel fibers, with an aspect ratio of 60, a tensile strength exceeding 600 MPa, and a mass density of 785 kg/m$^3$, were also incorporated. To improve workability, a high-performance polycarboxylate superplasticizer with a water-reducing rate of 30% was added during mixing process using regular tap water as the source for mixing water supply. Table 1 provides detailed information on the chemical composition of the cement and fly ash used in the experiment.

Table 1. Chemical composition of OPC and fly ash (%)

| **Constituent (wt.%)** | **$SiO_2$** | **$Al_2O_3$** | **CaO** | **MgO** | **$SO_3$** | **$Fe_2O_3$** |
|---|---|---|---|---|---|---|
| Cement | 19.5 | 4.76 | 64.68 | 2.16 | 3.02 | 3.25 |
| Fly ash | 50.72 | 28.78 | 6.93 | 1.21 | 1.26 | 4.23 |

The experimental SFRRC had a water-binder ratio of 0.45. Rubber particles were used to replace fine aggregate on a volume-to-volume basis, with a replacement ratio of 10%. The study examined the effect of varying steel fiber content by utilizing five test groups with volume fractions of 0, 0.5, 1.0, 1.5, and 2.0%. The mix proportions used in the SFRRC are listed in Table 2.

(The numbers following F represent the varying volume fractions of steel fibers, specifically 0, 0.5, 1.0, 1.5, and 2.0%.)

Table 2. Mix proportion of SFRRC /(kg/m$^3$)

| Sample types | Cement | Fly ash | Water | Aggregate | Sand | Rubber | Steel fiber | Superplas-ticizer |
|---|---|---|---|---|---|---|---|---|
| SF-0 | 366 | 41 | 183 | 1056 | 677 | 27.2 | 0 | 4.07 |
| SF-0.5 | 366 | 41 | 183 | 1056 | 677 | 27.2 | 39 | 4.07 |
| SF-1.0 | 366 | 41 | 183 | 1056 | 677 | 27.2 | 78 | 4.07 |
| SF-1.5 | 366 | 41 | 183 | 1056 | 677 | 27.2 | 117 | 4.07 |
| SF-2.0 | 366 | 41 | 183 | 1056 | 677 | 27.2 | 156 | 4.07 |

### 2.2. Testing methodologies

$Na_2SO_4$ solution with a mass fraction of 3% was used to simulate the sulfate environment. The rapid freeze-thaw test was conducted using prism specimens (100 mm × 100 mm × 400 mm) and cubic specimens (100 mm × 100 mm × 100 mm). After curing, the SFRRC test specimens were soaked in the $Na_2SO_4$ solution at room temperature for 4 days. Then, they were placed into the rapid freeze-thaw testing machine to initiate the test, following the procedures outlined in the literature [21]. The machine contains 28 rubber specimen containers, each capable of accommodating four cubic specimens or a single prism specimen. After placing the specimens, add $Na_2SO_4$ solution to the containers, ensuring that the liquid level is at least 5 mm above the top of the specimens.

Following each series of 50 freeze-thaw cycles, the prism specimens were utilized for measuring mass and RDME, while the cube specimens were utilized to assess compressive strength. The SFRRC damage layer was measured according to the literature [22] using the prism specimens. Based on the variation in ultrasonic wave velocity propagation in concrete with different degrees of compaction, the $H_f$ can be measured using an NM-4B non-metal ultrasonic testing device. According to the results of previous experimental studies [23, 24], measurement was conducted every 50 cycles, and finally stopped after 300 cycles. After each measurement, a fresh $Na_2SO_4$ solution is used to replace the current one in order to maintain the desired concentration for experimentation.

## 3. Results and discussion

### 3.1. Compressive strength

Figure 1 illustrates the compressive strength of SFRRC with different steel fiber contents prior to freeze-thaw cycles. Compared to SF-0, the compressive strength increases by 3.04%, 5.52%, 9.67%, and 7.18% for SF-0.5, SF-1.0, SF-1.5, and SF-2.0 respectively. It is evident that the incorporation of steel fibers enhances the compressive strength of rubberized concrete to a certain extent, thereby mitigating the adverse effect of rubber addition on the compressive strength of concrete. The appropriate amount of steel fibers can effectively exert their toughening

and crack resistance effects, positively contributing to the compressive strength of concrete. However, when the steel fiber content continues to increase, it often leads to an increase in interfaces between steel fibers and cement paste, which represent weakness areas in concrete prone to crack propagation [25]. These internal defects within the matrix ultimately impact the mechanical properties of SFRRC.

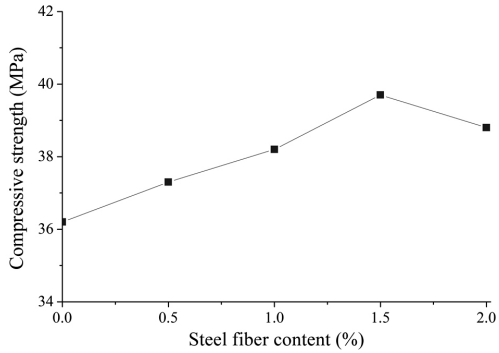


Fig. 1. Compressive strength of SFRRC before freeze-thaw test

## 3.2. Mass variation

Figure 2 illustrates the variation pattern of mass loss in SFRRC during the experiment. The mass loss of SFRRC occurs in two stages: a slow increase followed by a rapid increase. SF-0 experiences a rapid increase in mass loss after 150 cycles, representing the maximum mass loss. With the addition of steel fibers, the mass loss is noticeably reduced. Within the suitable range of steel fiber volume fraction, increasing the content causes the mass loss to gradually diminish. Among the specimens examined, SF-1.5 exhibited the smallest mass loss. However, when the steel fiber content reaches 2.0%, the mass loss increases significantly, indicating a decrease in the ability of the SFRRC to resist sulfate freeze-thaw-induced erosion. It is seen

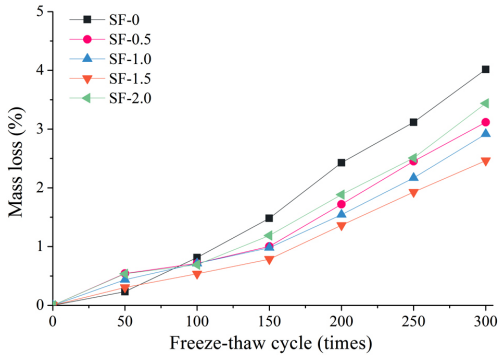


Fig. 2. Mass loss of SFRRC

that the addition of an appropriate amount of steel fiber to the rubberized concrete enhances its freeze-thaw resistance, a phenomenon that can be attributed to the fact that steel fibers can mitigate the damage caused by freeze-thaw expansion tensile stress during the cycling while increasing the splitting tensile strength of the SFRRC, thereby suppressing the generation and propagation of internal microcracks or defects.

## 3.3. Variation in RDME

Figure 3 shows the variation pattern of the RDME in SFRRC during the experiment.

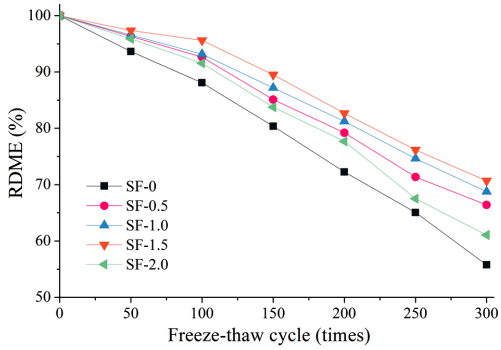


Fig. 3. RDME of SFRRC

It is seen that the process involves two stages: a slow reduction followed by a rapid reduction in the RDME. After 300 cycles, the RDMEs of SF-0, SF-0.5, SF-1.0, SF-1.5, and SF-2.0 decrease by 44.25, 33.59, 31.24, 29.31, and 38.94%, respectively. The RDME of SF-0 exhibits a rapid increase after 150 cycles, with a loss rate exceeding 40% after 300 cycles, indicating that the frost resistance is the poorest. As the steel fiber content gradually increases within a range of 0 to 1.5%, the loss rate of RDME decreases. Among the samples, SF-1.5 demonstrates superior frost resistance. However, it is observed that increasing the steel fiber content to 2.0% leads to a noticeable increase in RDME loss and subsequent decrease in frost resistance. At this content, agglomeration is prone to occur during the mixing process, which subsequently weakens the resistance to sulfate and freeze-thaw cycling.

## 3.4. Change in relative compressive strength

Figure 4 illustrates the variation pattern of in the relative compressive strength in SFRRC during the experiment. It is seen that the process involves two stages: a slow increase followed by a rapid increase. After 300 cycles, the relative compressive strengths of SF-0, SF-0.5, SF-1.0, SF-1.5, and SF-2.0 decrease to 63.26, 67.02, 72.25, 75.57, and 66.24%, respectively. The biggest relative compressive loss is found in the SF-0 sample. When the steel fiber content gradually increases in the range of 0–1.5%, the relative compressive strength loss rate gradually decreases. SF-2.0, which has the highest steel fiber content, shows an increase in compressive

strength loss rather than a decrease. These test results are consistent with the variation patterns of mass loss and RDME shown in Fig. 2 and Fig 3. It is seen that steel fibers, as reinforcement material, not only compensate for the reduction in concrete strength caused by the incorporation of rubber but also mitigate the loss of compressive strength in SFRRC under sulfate and freeze-thaw environments.

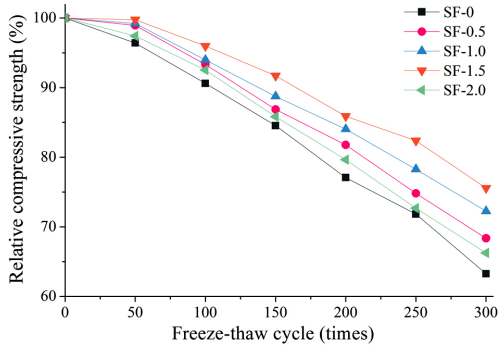


Fig. 4. Relative compressive strength of SFRRC

## 3.5. Change in damage layer thickness

Figure 5 shows the variation pattern of ultrasonic velocity and $H_f$ in SFRRC during the experiment. The results suggest that as the experiment progresses, there is a decrease in ultrasonic velocity and an increase in the $H_f$ in SFRRC. After 300 cycles, the ultrasonic velocities in the damage layers of SF-0, SF-0.5, SF-1.0, SF-1.5, and SF-2.0 drop by 31.99, 28.35, 25.77, 23.37, and 31.28%, respectively. The highest ultrasonic velocity loss rate is seen in the SF-0 specimen. From the graph, it is also evident that SF-0 exhibits the highest

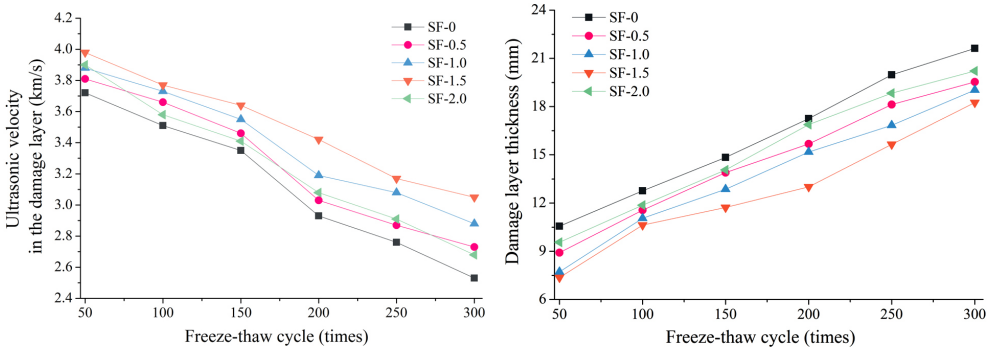


(a) (b)

Fig. 5. Change in damage layer thickness of SFRRC: (a) the ultrasonic velocity, (b) the $H_f$

$H_f$, indicating the most severe level of deterioration. The addition of steel fiber results in a reduction in the $H_f$ of SFRRC to a certain extent, leading to a thinner damage layer as the steel fiber content increases. At a content of 1.5%, the damage layer is thinnest and the resistance to sulfate erosion under freeze-thaw environment is highest. Among the four types of SFRRC examined, SF-2.0 has the thickest damage layer, demonstrating that a high steel fiber content will aggravate the deterioration of rubber concrete.

As depicted in Fig. 6, after 50 cycles, a correlation develops between the $H_f$ and the change rule of RDME revealed in Fig. 3. It is seen that, when the RDME of SF-0 reduces rapidly, the $H_f$ increases significantly; when the RDME of SF-1.5 declines the least, the $H_f$ increases the least, indicating where SF-1.5 experiences the minimum amount of deterioration. This finding indicates that the extent of damage and deterioration in SFRRC can be characterized through the measurement of the $H_f$.

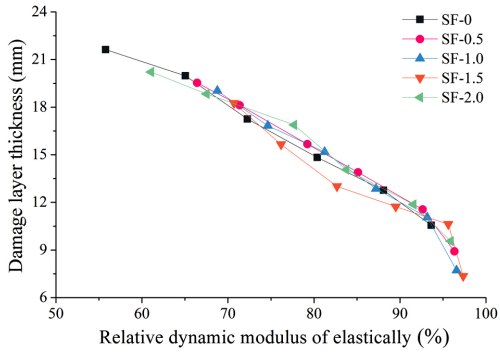


Fig. 6. Relationship between $H_f$ and RDME

## 4. Calculation of the compressive strength of damage layer

The gradual increase in $H_f$ leads to a decrease in both compactness and compressive strength of the damage layer, consequently resulting in a deterioration of the mechanical properties of SFRRC. SFRRC damaged by sulfate erosion and freeze-thaw cycling comprises an external damage layer and internal undamaged concrete. Assuming that these two components are evenly distributed, the compressive strength satisfies Eq. (4.1):

$$f_n A_n = f_{cn} A_{cn} + f_{dn} A_{dn} \tag{4.1}$$

Where $f_{cn}$, $f_{dn}$, and $f_n$ are, respectively, the compressive strengths of the undamaged SFRRC, the SFRRC in the damage layer, and the SFRRC after freeze-thaw cycling (comprising a damage layer and undamaged concrete), all measured in MPa; and $A_{cn}$, $A_{dn}$, and $A_n$ are, respectively, the sectional areas of the undamaged SFRRC, the SFRRC in the damage layer, and the SFRRC after freeze-thaw cycling (comprising a damage layer and undamaged concrete), all measured in mm$^2$, where $A_{cn} = (100 - 2H_f)^2$ mm$^2$, $A_{dn} = (A_n - A_{cn})$ mm$^2$, $A_n = 10^4$ mm$^2$.

Table 3 shows the calculated values of $f_{dn}$. After 300 cycles, the compressive strength losses in the damage layer of SF-0, SF-0.5, SF-1.0, SF-1.5, and SF-2.0 are 55.11, 51.58, 45.99, 42.29, and 53.48%, respectively. Compared to the test results depicted in Fig. 4, the $f_{dn}$ exhibits

Table 3. The compressive strength of concrete in the damage layer of SFRRC

| **Sample types** | **Freeze-thaw cycles** | $A_n$ /mm$^2$ | $A_{cn}$ /mm$^2$ | $A_{dn}$ /mm$^2$ | $f_n$ /MPa | $f_{cn}$ /MPa | $f_{dn}$ /MPa |
|---|---|---|---|---|---|---|---|
| SF-0 | 50 cycles | 10000 | 6222.05 | 3777.95 | 34.9 | 36.2 | 32.76 |
| | 100 cycles | 10000 | 5547.27 | 4452.73 | 32.8 | 36.3 | 28.44 |
| | 150 cycles | 10000 | 4947.72 | 5052.28 | 30.6 | 36.3 | 25.02 |
| | 200 cycles | 10000 | 4290.25 | 5709.75 | 27.9 | 36.5 | 21.44 |
| | 250 cycles | 10000 | 3607.20 | 6392.80 | 26.0 | 36.7 | 19.96 |
| | 300 cycles | 10000 | 3221.70 | 6778.30 | 22.9 | 36.9 | 16.25 |
| SF-0.5 | 50 cycles | 10000 | 6753.55 | 3246.45 | 36.9 | 37.3 | 36.07 |
| | 100 cycles | 10000 | 5910.53 | 4089.47 | 34.8 | 37.5 | 30.90 |
| | 150 cycles | 10000 | 5215.73 | 4784.27 | 32.4 | 37.5 | 26.84 |
| | 200 cycles | 10000 | 4714.20 | 5285.80 | 30.5 | 37.6 | 24.17 |
| | 250 cycles | 10000 | 4065.34 | 5934.66 | 27.9 | 37.9 | 21.05 |
| | 300 cycles | 10000 | 3713.68 | 6286.32 | 25.5 | 38.1 | 18.06 |
| SF-1.0 | 50 cycles | 10000 | 7150.39 | 2849.61 | 37.9 | 38.3 | 36.90 |
| | 100 cycles | 10000 | 6068.41 | 3931.59 | 35.9 | 38.3 | 32.20 |
| | 150 cycles | 10000 | 5517.52 | 4482.48 | 33.9 | 38.5 | 28.24 |
| | 200 cycles | 10000 | 4852.52 | 5147.48 | 32.1 | 38.6 | 25.97 |
| | 250 cycles | 10000 | 4401.00 | 5599.00 | 29.9 | 38.6 | 23.06 |
| | 300 cycles | 10000 | 3836.56 | 6163.44 | 27.6 | 38.8 | 20.63 |
| SF-1.5 | 50 cycles | 10000 | 7272.68 | 2727.32 | 39.6 | 39.8 | 39.07 |
| | 100 cycles | 10000 | 6199.99 | 3800.01 | 38.1 | 39.8 | 35.33 |
| | 150 cycles | 10000 | 5858.37 | 4141.63 | 36.4 | 39.8 | 31.59 |
| | 200 cycles | 10000 | 5473.04 | 4526.96 | 34.1 | 40.1 | 26.85 |
| | 250 cycles | 10000 | 4719.69 | 5280.31 | 32.7 | 40.2 | 26.00 |
| | 300 cycles | 10000 | 4032.25 | 5967.75 | 30.0 | 40.5 | 22.91 |
| SF-2.0 | 50 cycles | 10000 | 6541.57 | 3558.43 | 37.8 | 38.9 | 35.72 |
| | 100 cycles | 10000 | 5815.59 | 4184.41 | 35.9 | 38.9 | 31.73 |
| | 150 cycles | 10000 | 5166.73 | 4833.27 | 33.3 | 39.2 | 26.99 |
| | 200 cycles | 10000 | 4387.74 | 5612.26 | 30.9 | 39.2 | 24.41 |
| | 250 cycles | 10000 | 3886.28 | 6113.72 | 28.2 | 39.5 | 21.02 |
| | 300 cycles | 10000 | 3549.78 | 6450.22 | 25.7 | 39.6 | 18.05 |

a more significant decrease, indicating a severe deterioration in the damage layer. The loss rate of $f_{dn}$ in the SF-0 is the highest. As the steel fiber content increases within a range of 0 to 1.5%, the loss rate of $f_{dn}$ in SFRRC gradually decreases. Under the influence of environmental factors, damage first appears in the damage layer. However, the random distribution of steel fibers can effectively inhibit the expansion of cracks within the damage layer, thereby slowing down the loss of compressive strength in this layer.

The $f_{dn}$ under the influence of environmental factors is a part of the overall compressive strength of SFRRC. There exists a correlation between these two compressive strengths that can be used to obtain a relationship through curve fitting, as shown in Fig. 7. Mathematically, this relationship is given by Eq. (4.2):

$$f_{dn} = 0.065 f_n^{1.733} \tag{4.2}$$

Eq. (4.2) can be conveniently applied to calculate the $f_{dn}$ of SFRRC under sulfate erosion in a freeze-thaw environment, thereby providing a basis for determining the load-bearing capacity of SFRRC influenced by environmental factors.

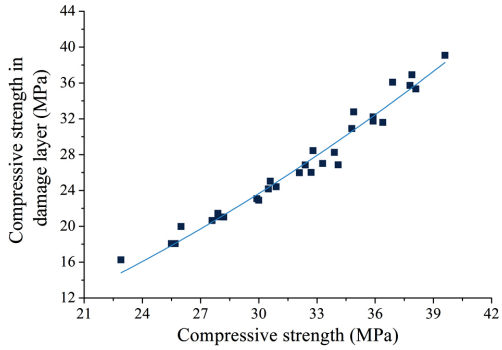


Fig. 7. Relationship between $f_{dn}$ and $f_n$ of SFRRC

## 5. Analysis of the pore structure in SFRRC

The mercury intrusion porosimetry method was used to evaluate the pore structural parameters of SFRRC specimens. The samples are cement mortar particles, with aggregates removed; each particle measures approximately 5 mm in diameter. As detailed in Table 4, a noticeable trend emerges: as the steel fiber content gradually increases from 0 to 1.5%, there are corresponding decreases in the total porosity, total pore volume, and total pore area of the SFRRC. This indicates that incorporating an appropriate amount of steel fibers has a beneficial effect on the pore structure of rubber concrete, with the most favorable results occurring when the steel fiber content reaches 1.5%. Relative to SF-0 without steel fibers, SF-1.5 experiences a reduction of 26.75% in total porosity and decreases of 26.96% in total pore volume and 37.75% in total pore area. Additionally, both the average and most probable pore diameters are

also reduced in SF-1.5. The reason is that shrinking occurring as a result of water loss and other factors during the molding and curing process of SFRRC. When the shrinkage stress reaches the tensile strength of the concrete, microcracks of varying scales appear within the concrete. An appropriate steel fiber content can effectively keep such cracks from growing, reducing the number and size of microcracks and creating a more reasonable pore structure in the SFRRC.

Table 4. Pore structure parameters of SFRRC with different steel fiber contents

| **Sample types** | **Total porosity /%** | **Total pore volume /(ml/g)** | **Total pore area /($m^2$/g)** | **Critical pore diameter /nm** | **Average pore diameter /nm** | **Most probable pore diameter /nm** |
|---|---|---|---|---|---|---|
| SF-0 | 18.28 | 0.0905 | 28.21 | 46.29 | 58.16 | 65.43 |
| SF-0.5 | 17.23 | 0.0839 | 24.35 | 36.31 | 41.79 | 46.63 |
| SF-1.0 | 15.75 | 0.0756 | 21.13 | 31.69 | 34.15 | 37.71 |
| SF-1.5 | 13.39 | 0.0661 | 17.56 | 25.56 | 26.78 | 30.35 |
| SF-2.0 | 17.66 | 0.0835 | 25.57 | 41.03 | 46.51 | 52.91 |

When the content reaches 2.0%, however, a varying degree of increase occurs in the pore structure parameters of SFRRC. Compared with SF-1.5, the total porosity, total pore volume, and total pore area of SF-2.0 increase by 31.89, 26.32, and 45.62%, respectively. The mean and most-probable pore-sizes also increase significantly. These increases occur because the addition of a high amount of steel fibers results in fiber agglomeration during concrete mixing. Consequently, this increases the probability of honeycomb and pitted surfaces forming on the SFRRC, ultimately leading to an increase in porosity and larger pores.

Figure 8 illustrates the distribution of pore sizes in SFRRC. It is seen that increasing the steel fiber content (from 0 to 1.5%) causes the volume fraction of pore-sizes within the $d < 20$ nm and 20 nm $\leq d <$ 50 nm ranges to gradually increase, with the fraction within the range

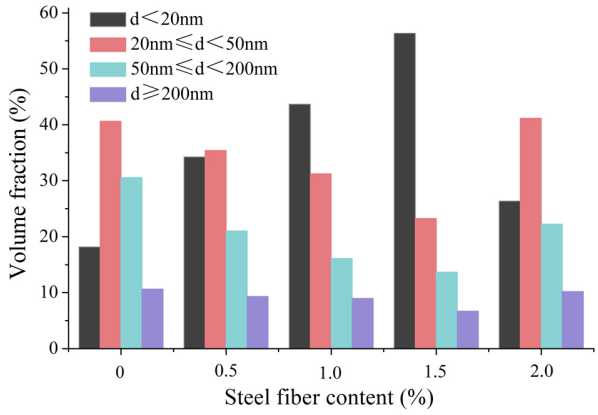


Fig. 8. The influence of steel fiber content on the distribution of pore size

$d < 20$ increasing significantly and those within the 50 nm $\leq d <$ 200 nm and $d \geq 200$ nm ranges decreases gradually. These experimental results align with the trends in macroscopic physical property changes depicted in Figs. 2 to 4. The incorporation of an appropriate quantity of steel fibers facilitates the formation of harmless or less harmful pores and micro-pores in concrete, while simultaneously reducing the presence of harmful or more harmful pores. This improvement in pore structure proves beneficial for improving the mechanical properties and sulfate frost resistance of SFRRC. However, as the steel fiber content increases to 2.0%, the quantities of harmful and more harmful pores increase noticeably, leading to a decrease in the freeze-thaw resistance for SF-2.0.

# 6. Conclusions

1. As the freeze-thaw experiment progresses, the mass loss of SFRRC initially increases slowly and then rapidly, while the RDME and compressive strength decrease slowly at first and then rapidly. As the $H_f$ continues to grow and the ultrasonic velocity in the damage layer decreases gradually, resulting in a significant loss of compressive strength of this layer.
2. A calculation method for the compressive strength of the damage layer is established based on the $H_f$ and the compressive strength of SFRRC after degradation, providing a basis for calculating the bearing capacity of SFRRC under the influence of environmental factors.
3. The incorporation of steel fibers enhances the frost resistance of rubber concrete. As the proportion of steel fibers increases from 0 to 1.5%, the SFRRC exhibits a decrease in total porosity, pore volume, and pore area, simultaneously enhancing the proportion of harmless pores and optimizing the pore structure. The frost resistance of SFRRC gradually improves in sulfate solution, with SF-1.5 demonstrating the best performance.
4. When the fiber content reaches 2.0%, there is an increase in the number of harmful and more harmful pores, resulting in a deterioration of the pore structure. The frost resistance of SF-2.0 experiences a significant decrease, but it is still better than SF-0 without steel fibers.

## Acknowledgements

This project was supported by Key Scientific and Technology Project of Henan Province (232102320192, 242102320370, 212102310091); Key Scientific Research Project of Higher Education Institutions in Henan Province (24B560002); Anyang Key R&D and Promotion Project (2023C01SF007).

## References

[1] J. Xu, Z.Y. Yao, G. Yang, and Q.H. Han, "Research on crumb rubber concrete: From a multi-scale review", *Construction and Building Materials*, vol. 232, art. no. 117282, 2020, doi: 10.1016/j.conbuildmat.2019.117282.

[2] K. Walotek, J. Bzówka, and A. Ciołczyk, "Selected issues concerning the use of Shredded Rubber Waste (SRW) in binder-bound mixtures", *Archives of Civil Engineering*, vol. 70, no. 2, pp. 79–95, 2024, doi: 10.24425/ace.2024.149852.

[3] K. Bisht and P.V. Ramana, "Evaluation of mechanical and durability properties of crumb rubber concrete", *Construction and Building Materials,* vol. 155, pp. 811–817, 2017, doi: 10.1016/j.conbuildmat.2017.08.131.

[4] R. Roychand, R.J. Gravina, Y. Zhuge, X. Ma, O. Youssf, and J.E. Mills, "A comprehensive review on the mechanical properties of waste tire rubber concrete", *Construction and Building Materials*, vol. 237, art. no. 117651, 2020, doi: 10.1016/j.conbuildmat.2019.117651.

[5] S. Guler, Z.F. Akbulut, H. Siad, and M. Lachemi, "Enhanced freeze-thaw resilience of cement mortars through Nano-$SiO_2$ and single/hybrid basalt fiber incorporation: Assessing workability, strength, durability", *Journal of Building Engineering*, vol. 89, art. no. 109177, 2024, doi: 10.1016/j.jobe.2024.109177.

[6] S. Guler and Z.F. Akbulut, "Workability, physical & mechanical properties of the cement mortars strengthened with metakaolin and steel/basalt fibers exposed to freezing-thawing periods", *Construction and Building Materials*, vol. 394, art. no. 132100, 2023, doi: 10.1016/j.conbuildmat.2023.132100.

[7] Q.H. Zhao, S. Dong, and H. Zhu, "Experiment on stress-strain behavior and constitutive model of steel fiber-rubber/ concrete subjected to uniaxial compression", *Acta Materiae Compositae Sinica*, vol. 38, no. 7, pp. 2359–2369, 2021, doi: 10.13801/j.cnki.fhclxb.20200916.001.

[8] J.Q. Wang, Q.L. Dai, R.Z. Si, Y.X. Ma, and S.C. Guo, "Fresh and mechanical performance and freeze-thaw durability of steel fiber-reinforced rubber self-compacting concrete (SRSCC)", *Journal of Cleaner Production*, vol. 277, art. no. 123180, 2020, doi: 10.1016/j.jclepro.2020.123180.

[9] C.Q. Fu, H.L. Ye, K.J. Wang, K. Zhu, and C. He, "Evolution of mechanical properties of steel fiber-reinforced rubberized concrete (FR-RC)", *Composites Part B: Engineering*, vol. 160, pp. 158–166, 2019, doi: 10.1016/j.compositesb.2018.10.045.

[10] N. Nan, "Prediction of concrete life under coupled dry and wet-sulfate erosion based on damage evolution equation", *Archives of Civil Engineering*, vol. 69, no. 4, pp. 679–692, 2023, doi: 10.24425/ace.2023.147683.

[11] Y.F. Li, J.L. Li, T.Y. Guo, T.F. Zhao, L.S. Bao, and X.L. Sun, "Bearing capacity and seismic performance of Y-shaped reinforced concrete bridge piers in a freeze-thaw environment", *Archives of Civil Engineering*, vol. 69, no. 1, pp. 367–384, 2023, doi: 10.24425/ace.2023.144178.

[12] N.-P. Pham, A. Toumi, and A. Turatsinze, "Evaluating damage of rubberized cement-based composites under aggressive environments", *Construction and Building Materials*, vol. 217, pp. 234–241, 2019, doi: 10.1016/j.conbuildmat.2019.05.066.

[13] W. Zeng, Y. Ding, Y.L. Zhang, and D. Frank, "Effect of steel fiber on the crack permeability evolution and crack surface topography of concrete subjected to freeze-thaw damage", *Cement and Concrete Research*, vol. 138, art. no. 106230, 2020, doi: 10.1016/j.cemconres.2020.106230.

[14] C.Q. Liu, J.L. Sun, X.R. Tang, and Y.H. Ma, "The durability of spray steel fiber-reinforced recycled coarse aggregate concrete", *Construction and Building Materials*, vol. 412, art. no. 134731, 2024, doi: 10.1016/j.conbuildmat.2023.134731.

[15] T. Gonen, "Freezing-thawing and impact resistance of concretes containing waste crumb rubbers", *Construction and Building Materials*, vol. 177, pp. 436–442, 2018, doi: 10.1016/j.conbuildmat.2018.05.105.

[16] A. Richardson, K. Coventry, V. Edmondson, and E. Dias, "Crumb rubber used in concrete to provide freeze thaw protection (optimal particle size)", *Journal of Cleaner Production*, vol. 112, pp. 599–606, 2016, doi: 10.1016/j.jclepro.2015.08.028.

[17] A. Alsaif, S.A. Bernal, M. Guadagnini, and K. Pilakoutas, "Durability of steel fibre reinforced rubberised concrete exposed to chlorides", *Construction and Building Materials*, vol. 188, pp. 130–142, 2018, doi: 10.1016/j.conbuildmat.2018.08.122.

[18] A. Alsaif, S.A. Bernal, M. Guadagnini, and K. Pilakoutas, "Freeze-thaw resistance of steel fibre reinforced rubberised concrete", *Construction and Building Materials*, vol. 195, pp. 450–458, 2018, doi: 10.1016/j.conbuildmat.2018.11.103.

[19] T. Luo, C. Zhang, C. W. Sun, X.C. Zheng, Y.J. Ji, and X.S. Yuan, "Experimental investigation on the freeze-thaw resistance of steel fibers reinforced rubber concrete", *Materials*, vol. 13, no. 5, art. no. 1260, 2020, doi: 10.3390/ma13051260.

[20] A.J. Chen, J. Wang, and Y. Ma, "Test of frost resistance for steel fiber rubber recycled concrete", *Acta Materiae Compositae Sinica*, vol. 32, no. 4, pp. 933–941, 2015, doi: 10.13801/j.cnki.fhclxb.20141022.006.

[21] GB/T 50082-2009 Standard for Test Method of Long-term Performance and Durability of Ordinary Concrete. National Standard of the People's Republic of China, 2009.

[22] CECS 21:2000 Technical Specification for Inspection of Concrete Defects by Ultrasonic Method. Standard of China Engineering Construction Standardization Association, 2000.

[23] L. Jiang and D.T. Niu, "Damage degradation law of concrete in sulfate solution and freeze-thaw environment", *Journal of Central South University Science and Technology*, vol. 47, no. 9, pp. 3208–3216, 2016.

[24] L. Jiang and D.T. Niu, "Study on constitutive relation of concrete under sulfate attack and freeze-thaw environment", *Advanced Engineering Sciences*, vol. 48, no. 3, pp. 71–78, 2016, doi: 10.15961/j.jsuese.2016.03.009.

[25] J.B. Wang, D.T. Niu, Y. Wang, and B. Wang, "Durability performance of brine-exposed shotcrete in salt lake environment", *Construction and Building Materials*, vol. 188, pp. 520–536, 2018, doi: 10.1016/j.conbuildmat.2018.08.139.

Received: 2024-05-24, Revised: 2024-08-27